# OPTIMISATION OF PULVERISED COAL COMBUSTION BY MEANS OF CFD/CTA MODELLING

by

## Risto V. FILKOSKI, Ilija J. PETROVSKI, and Piotr KARAS

*The objective of the work presented in this paper was to apply a method for handling two-phase reacting flow for prediction of pulverised coal combustion in large-scale boiler furnace and to assess the ability of the model to predict existing power plant data. The paper presents the principal steps and results of the numerical modelling of power boiler furnace with tangential disposition of the burners. The computational fluid dynamics/computational thermal analysis (CFD/CTA) approach is utilised for creation of a three-dimensional model of the boiler furnace, including the platen superheater in the upper part of the furnace. Standard k-ε model is employed for description of the turbulent flow. Coal combustion is modelled by the mixture fraction/probability density function approach for the reaction chemistry, with equilibrium assumption applied for description of the system chemistry. Radiation heat transfer is computed by means of the simplified P-N model, based on the expansion of the radiation intensity into an orthogonal series of spherical harmonics.*

*Some distinctive results regarding the examined boiler performance in capacity range between 65 and 95% are presented graphically. Comparing the simulation predictions and available site measurements concerning temperature, heat flux and combustion efficiency, a conclusion can be drawn that the model produces realistic insight into the furnace processes. Qualitative agreement indicates reasonability of the calculations and validates the employed sub-models. After the validation and verification of the model it was used to check the combustion efficiency as a function of coal dust sieve characteristics, as well as the impact of burners modification with introduction of over fire air ports to the appearance of incomplete combustion, including CO concentration, as well as to the $NO_x$ concentration.*

*The described case and other experiences with CFD/CTA stress the advantages of numerical modelling and simulation over a purely field data study, such as the ability to quickly analyse a variety of design options without modifying the object and the availability of significantly more data to interpret the results.*

Key words: *CFD modelling, pulverised coal-fired boiler, combustion, thermal radiation, heat transfer, furnace*

## Introduction

Efficient use of pulverised coal in boilers with tangential burners system is crucial to the power generation in the most Southeastern European countries, which was the

main motivation for undertaking this research. Current revitalisation and modernisation of pulverised coal-fired boilers mainly concerns modification of furnaces, restoration of the milling system, installation of low-$NO_x$ burners and over fire air (OFA) ports. Price competition and emission limits are forcing the power plant owners and operators to improve the efficiency and cleanliness of the combustion systems. In most cases, the modifications are so complex that their impact on boiler performance cannot be predicted without proper state-of-the-art modelling tools. Also, by its nature, the combustion process of pulverised coal in boiler furnace is an example of very complex turbulent flow, accompanied by strong coupling of mass, momentum and energy in two phases.

Numerical simulation techniques through the last decades have grown from being promising, mainly scientific tool, to a basic technology, unavoidable in engineering practice. Simulations made with proper numerical models using the computational fluid dynamics and computational thermal analysis (CFD/CTA) offer great potential in analysing, designing, retrofitting and optimising performances of fossil-fuel power systems. Such approach enables engineers and researchers to virtually make design changes and draw conclusions regarding possible consequences. Compared with other computational methods, CFD/CTA modelling provides researchers with detailed insight into the performance characteristics of the investigated object, giving better and more-accurate representations of combustion system's geometry, physics and chemistry at affordable cost. Thus, it is becoming a very efficient tool in efforts to meet strict combustion system's operation and performance goals.

Three-dimensional models of industrial and utility scale combustion systems, including models of tangentially fired furnaces, have been developed and successfully applied for years now [1-13]. Such models are often similar to each other in many ways and the majority use variations of the SIMPLE algorithm for coupling of velocity and pressure and the $k$-$\varepsilon$ gas turbulence model, or some derivatives, like RNG $k$-$\varepsilon$ model [4], or $k$-$\varepsilon$-$k_p$ two-phase turbulence model [10]. Gas phase conservation equations are mostly time-averaged and two-phase flow, as the one occurring in pulverised coal boilers, is usually described by Eulerian-Lagrangian approach and PSI-CELL method for taking into account the influence between phases, with some exceptions using Eulerian-Eulerian approach or two-fluid trajectory model. Most of the combustion submodels given in [3, 4, 7, 9-11, 13] separately treat particle devolatilisation, char oxidation and additional gas phase reactions. Thermal radiation is modelled by means of various approaches, like discrete transfer method, discrete ordinates method [7, 10, 11], six-fluxes method [9], Monte Carlo method [4], or so-called P-N model [14], as in this paper. Commercial CFD codes are applied successfully [2, 3, 11-13], but also research efforts are given worldwide to models specially developed for simulation of furnaces. It should be emphasized that a comprehensive model of the furnace processes must balance sub-model sophistication with computational practicality.

## Boiler design data and operating conditions

The utility boiler OB-380, analysed as a test case in this study [15, 16], designed and manufactured by RAFAKO S. A., Raciborz, Poland, is located at the 120 MW ther-
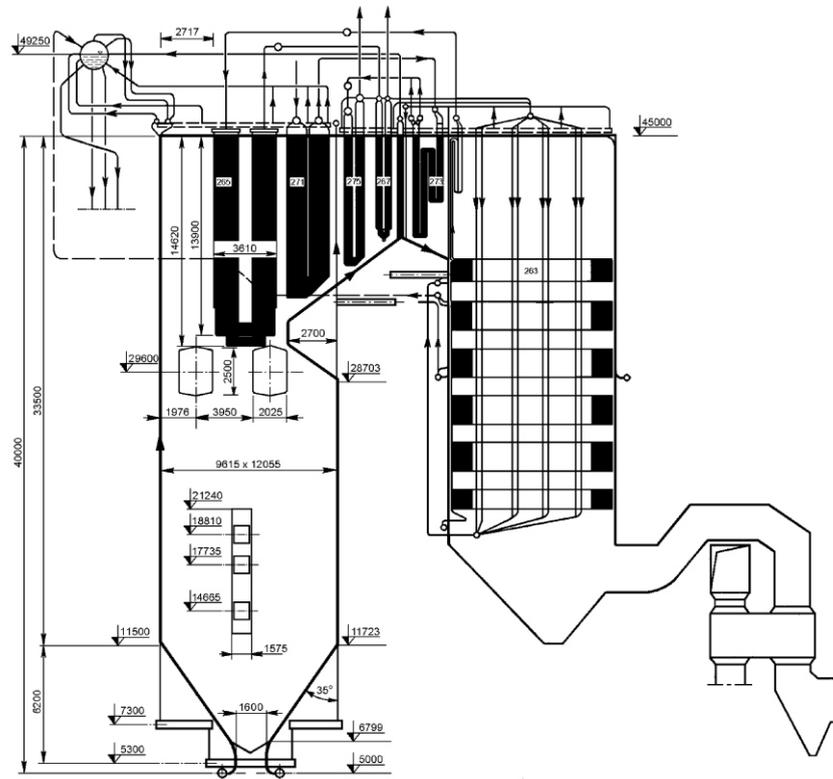
**Figure 1. Scheme of the utility boiler OB-380, TPP "Oslomej", Kicevo, Macedonia**

mal power plant "Oslomej" – Kicevo, Macedonia. Simplified configuration of the boiler, with the main dimensions of the furnace, is displayed in fig. 1 and the principal design technical characteristics are listed in tab. 1. The boiler silhouette is conventional, " " shaped. Membrane walls form the furnace, crossover pass and a part of the convective pass. The furnace is 12.055 m wide, 9.615 m long and approximately 40.0 m high. Six burners

**Table 1. Main characteristics of the boiler OB-380**

| Property | Value |
|---|---|
| Water-steam circulation | natural |
| Steam output | 105.6 kg/s |
| Parameters of superheated steam | 138 bar / 540 °C |
| Parameters of reheated steam | 27.7 bar / 540 °C |
| Parameters of feed water | 165 bar / 230 °C |
| Pressure in the boiler drum | 154 bar |
| Temperature of preheated air | 260 °C |
| Flue gases outlet temperature | 150 °C |
| Boiler efficiency | 85-88% |

163

for pulverised coal are arranged in such manner, as shown in fig. 2, to generate swirling flow of gas-solid mixture. Two of the burners are installed on the front, two on the back furnace wall and one on each sidewall. The boiler has already expanded its design operational lifetime, working very often at maximum capacity.
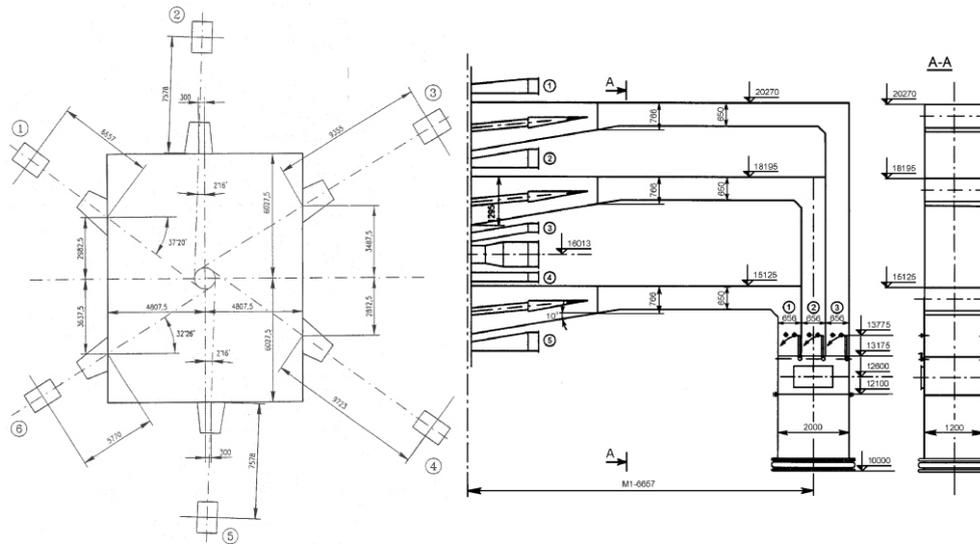


**Figure 2. Position of the burners in the furnace and burner vertical cross-section**

The boiler is fired with low-grade coal, lignite from the near-by coalmine, with huge content of ballast materials and with calorific value varying in broad range between 6500-8800 kJ/kg. Typical average proximate and ultimate analyse of the coal are given in tab. 2. Average coal consumption of the boiler operated at full load is 45-52 kg/s, while flue gases outflow in that case is approximately 160-200 m³/s.

**Table 2. Proximate and ultimate analysis of the Oslomej lignite (average values)**

| Proximate  analysis [%] | | Ultimate analysis [%] | |
|---|---|---|---|
| Char | 29.15 | C | 23.45 |
| Volatiles | 21.35 | H | 2.11 |
| $C_{fix}$ | 13.38 | O | 7.50 |
| Ash | 15.77 | N | 1.10 |
| Moisture | 49.50 | S | 0.57 |

The simulations in this study are performed in accordance to the present status of the boiler, which means, with the existing burner system disposition. Three basic cases of operating modes are subject of consideration in the article: working mode R1 corresponding to 83% boiler load (100 MW electrical output) with five burners in service,

164

modes R2 and R3 conducted on the basis of almost full load (115 MW electrical output) and modes R4 and R5 that correspond to 67% load. Values of the boiler parameters and operating conditions at modes R1 to R5 are presented in tab. 3 [15].

**Table 3. Boiler parameters at three different operating regimes [15]**

| Property | Mode R1 | Mode R2 | Mode R3 | Mode R4 | Mode R5 |
|---|---|---|---|---|---|
| Electrical output [MW] | 99.5 | 113.4 | 114.0 | 80.2 | 80.8 |
| Heat output [MW] | 269.5 | 300.7 | 312.3 | 215.5 | 214.5 |
| Steam production [kg/s] | 86.8 | 97.5 | 95.0 | 65.3 | 68.3 |
| Fuel consumption [kg/s] | 36.1 | 42.4 | 43.3 | 30.8 | 30.6 |
| Boiler efficiency [%] | 87.45 | 86.41 | 87.79 | 84.44 | 83.85 |
| Temperature of flue gases at boiler outlet [°C] | 156 | 166 | 142 | 147 | 161 |
| $CO_2/O_2$ in flue gases at the boiler outlet [%] | 10.94/8.68 | 12.38/6.95 | 11.95/7.35 | 8.41/10.94 | 8.34/11.02 |
| Temperature of preheated air [°C] | 206 | 215 | 185 | 195 | 219 |
| Excess air coefficient ahead of the air heaters | 1.415 | 1.295 | 1.345 | 1.965 | 1.985 |
| Burner out of service | No. 4 | No. 3 | No. 3 | No. 3 | No. 3 |

## Description of the applied model

CFD modelling consists of solution of governing equations for fluid flow, heat and mass transfer, radiation, chemical reactions, including combustion and other modelling equations. The equations are solved at several hundreds of thousands discrete points of numerical grid, in the previously defined computational domain. When the process involves flow of more than one phase, *i. e.* gas and solid particles, one approach is to model the process by solving a set of Navier-Stokes equations for the major phase, and to treat the minor phase as a set of discrete particles or droplets, which are tracked individually. This approach, Eulerian for gaseous and Lagrangian for discrete phase, is appropriate when the volume fraction of the discrete phase is low, such as in the case of pulverised coal combustion and, consequently, it is used in this research.

General structure of the case set-up and solution using the CFD/CTA technique is presented in fig. 3 [17]. Gambit pre-processor is used for geometry creation and mesh gener-
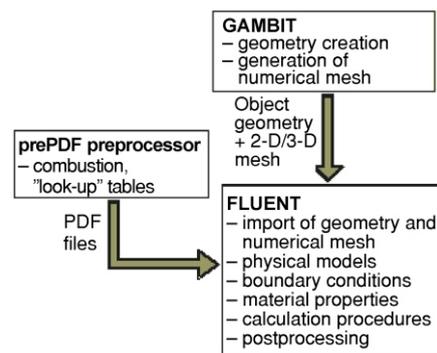


**Figure 3. Structure of the case set-up and solution with the CFD technique in the case of Fluent CFD package [17]**

ation, which is presented in fig. 4. Numerical mesh of 124839 finite volume cells, 375573 faces, and 125880 nodes is employed during the investigation. Some previous CFD simulations of this boiler unit, conducted with much denser numerical mesh, have given similar results to those presented in this article, but the CPU demand was much higher. The CFD software Fluent and prePDF pre-processor are employed for description of turbulent fluid flow, devolatilization, coal combustion, gas phase chemical reactions, and heat transfer. The simulations are performed for steady-state operating conditions, in a 3-D domain representing the full volume of the boiler furnace.



(a)                                    (b)                                    (c)
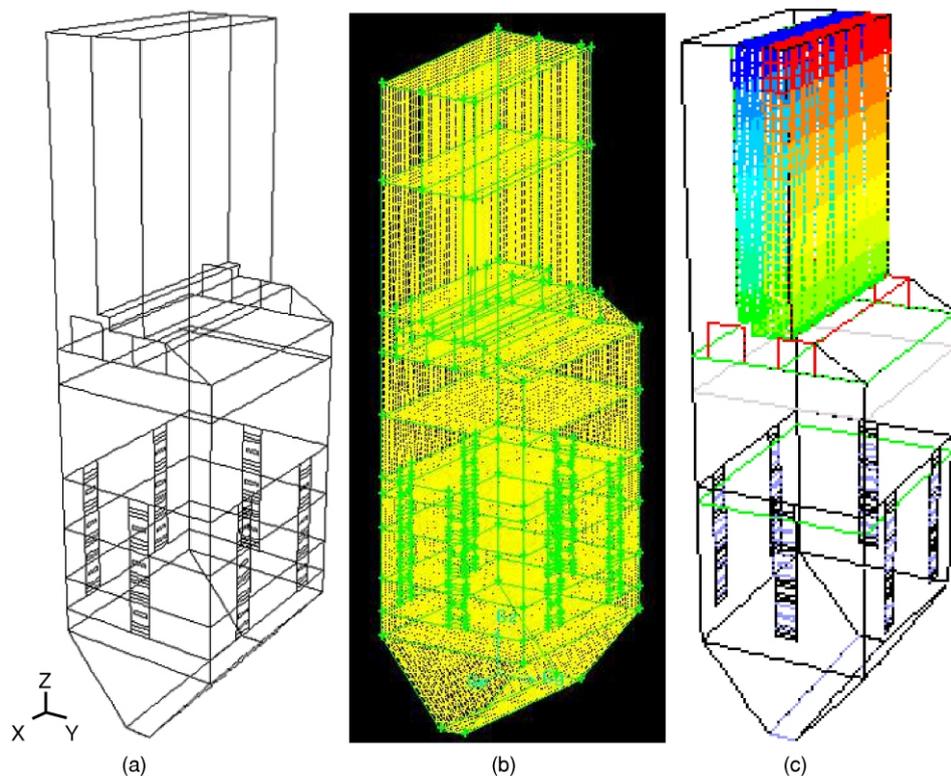
**Figure 4. Boiler furnace geometry: (a) feature, (b) finite-volume mesh, and (c) superheater zone (color image see on our web site)**

Turbulent mixing in the furnace was taken into account with the standard steady $k$-$\varepsilon$ model. Common values of the constants are used in the transport equations: $\sigma_k = 1.0$, $\sigma_\varepsilon = 1.3$, $C_{1\varepsilon} = 1.44$, and $C_{2\varepsilon} = 1.92$. Coupling of the continuity and momentum

166

equations is achieved by the SIMPLEC algorithm. Stochastic tracking model is used in the calculations to take the effects of turbulence on the particle trajectories into account. Mass flow rate, temperature, and mixture fraction is assigned at coal and air inlets, while outflow is prescribed at the recirculating holes and at the furnace exit, which, in this test case is located after the platen superheater. The superheater is modelled with parametric heat exchanger model to account for the heat absorption and pressure loss [15, 17]. For that purpose, a separate fluid zone is defined to represent the superheater core (fig. 4c), which is subdivided into macroscopic cells ("macro cells") along the coolant path [15]. The coolant inlet temperature to each macro cell is computed and then subsequently used to compute the heat rejection from each macro cell. This approach provides a realistic heat rejection distribution over the heat exchanger core. Soot formation and emission of pollutants, such as $NO_x$, is taken into consideration in the current steps of the investigation.

Numerical simulation of pulverised coal combustion involves modelling of continuous gas phase flow field and its interaction with a discrete phase of coal particles, which have non-uniform size distribution, with diameters ranging from 0 to 1000 m. The polydisperse particle size distribution is assumed to fit the Rosin-Rammler equation with a mean diameter $d_{pm}$ = 90-120 m and a spread parameter of 3.5.

The coal particles, carried by air-gas mixture, devolatilise and undergo char combustion, creating a source of fuel for reaction in the gas phase. The coal particle energy balance is used to calculate the particle temperature and to describe the coal evolution. In this test case, two-competing-kinetic-rates model is selected as a devolatilisation model. Combustion of pulverised coal is modelled as non-premixed kinetics/diffusion-limited process with the mixture-fraction/probability density function (PDF) approach for the reaction chemistry [17, 18]. Full equilibrium chemistry is selected as a chemistry model and the turbulence-chemistry interaction is modelled with a $\beta$ probability density function. It is assumed that the PDF mixture consists of 16 volumetric species: C(S), C, H, O, N, $O_2$, $N_2$, $CO_2$, $H_2O$, $H_2O(L)$, $CH_4$, $H_2$, CO, OH, NO, and HCN. Coal particle trajectory data, coal devolatilisation and combustion parameters used in the model are given in tabs. 4 and 5. Recirculation of the flue gases through holes in the upper part of the furnace (fig. 1) is included in the computations with a coefficient $r_g$ = 0.25-0.31, depending on the working mode.

One of the important issues in the case of coal combustion modeling is inclusion of the effect of discrete phase presence on the radiation absorption coefficient. The basic radiative transfer equation for an absorbing, emitting and scattering medium with contribution of the particulate phase, at position **r** in direction **s** is:

**Table 4. Coal particle trajectory data**

| | |
|---|---|
| Number of particle stream start locations | 18 |
| Maximum number of steps in each trajectory | – |
| Trajectory | 700 |
| Length scale | 0.1 m |
| Number of particle diameters | 8 |

$$\frac{dI(\mathbf{r,s})}{ds} \quad (a \quad a_p \quad s_p)I(\mathbf{r,s})$$

$$an^2 \frac{T^4}{} \quad E_p \quad \frac{\sigma_p}{4} \int_0^4 I(\mathbf{r,s})\Phi(\mathbf{s \quad s})d\Omega \quad (1)$$

167

**Table 5. Coal combustion parameters**

| (a) Coal devolatilisation data | | (b) Combusting particles properties | |
|---|---|---|---|
| Devolatilisation model – two competing rates | | Density | 1250 kg/m$^3$ |
| (1) First rate | | Specific heat capacity – picewise-linear profile | |
| – pre-exponential factor | 2.0 10$^5$ s$^{-1}$ | Thermal conductivity | 0.05 W/mK |
| – activation energy | 7.50 10$^7$ J/kmol | Mechanism factor | 2 |
| – weighting factor | 0.3 | Binary diffusivity | 4 10$^{-5}$ m$^2$/s |
| (2) Second rate | | Particle emissivity | 0.8 |
| – pre-exponential factor | 1.3 10$^7$ s$^{-1}$ | Particle scattering factor | 0.5 |
| – activation energy | 1.45 10$^8$ J/kmol | Swelling coefficient | 1.0 |
| – weighting factor | 1.0 | Mass diffusion limited rate constant | 5.0 10$^{-12}$ |
| | | Kinetic rate pre-exponential factor | 0.002 |
| | | Activation energy | 9.5 10$^7$ J/kmol |

where $I$ is total radiation intensity, which depends on position **r** and direction **s,** $s$ is path length, $a_p$ is the equivalent absorption coefficient due to the presence of particulates, $\sigma_p$ is equivalent particle scattering factor, $E_p$ is the equivalent particle emissivity, $a$ is absorption coefficient, $n$ is refractive index, $\sigma$ is Stefan-Boltzmann constant, $T$ is local absolute temperature, **s'** is scattering direction vector, $\Phi$ is phase function and ' is solid angle. The product $(a + \sigma_s)s$ is optical thickness or opacity of the medium.

In this work, radiation is taken into account in the heat transfer simulations through the so-called P-1 model [14, 17], based on expansion of the radiation intensity $I$ into an orthogonal series of spherical harmonics [14, 19, 20]. If only four terms in the series are used, the following equation is obtained for the radiation flux:

$$q_r \quad \frac{1}{3(a \quad \sigma_s) \quad C_{\sigma_s}} \quad G \tag{2}$$

where $G$ is incident radiation, $\sigma_s$ is scattering coefficient, and $C$ is linear-anisotropic phase function coefficient. Variable absorption coefficient $a$ is computed by the weighted-sum-of-gray-gases model (WSGGM) [17, 20-22].

The P-1 model has several advantages over other radiation models, treating the radiative transfer equation (1) as an easy-to-solve diffusion equation. Also, it is relatively simple, it can be easily applied to complicated geometries and it works reasonably well for combustion applications where the optical thickness is large. The particle emissivity, reflectivity, and scattering can be effectively included in the calculation of the radiation heat transfer.

The transport equation for $G$ is:

$$(\Gamma \ G) + 4\pi \quad a\frac{T^4}{} \quad E_p \quad (a \quad a_p)G \quad 0 \tag{3}$$

in which the parameter $\Gamma$ is defined through the equivalent absorption coefficient $a_p$ and the equivalent particle scattering factor $\sigma_p$:

$$\Gamma \quad \frac{1}{3(a \quad a_p \quad \sigma_p)} \tag{4}$$

With substitution $q_r = \ \Gamma \ G$ in eq. (3) the following expression is obtained for $q_r$:

$$q_r \quad 4 \quad a\frac{T^4}{} \quad E_p \quad (a \quad a_p)G \tag{5}$$

which can be directly included into the energy equation to account for heat sources due to radiation.

The flux of the incident radiation at wall $q_{rw}$ is determined with the expression:

$$q_{rw} \quad \frac{\varepsilon_w}{2(2 \quad \varepsilon_w)}(4 \ T_w^4 \quad G_w) \tag{6}$$

where $\varepsilon_w$ is wall emissivity, $T_w$ is wall temperature, and $G_w$ is incident wall radiation. The wall emissivity in this test case is specified in the range 0.65 to 0.8 at the furnace walls and 1.0 at the furnace bottom and exit. Sidewall temperature is calculated on a basis of the near-wall heat transfer conditions.

## Model evaluation and discussion

The 3-D CFD modelling approach of the combustion systems provides researchers with a more detailed understanding of the performance characteristics of the investigated object. Furthermore, it is becoming a very efficient tool in efforts to meet strict boiler's operation and performance goals. The main results of the performed CFD simulation concerning the OB-380 boiler consist of flow fields, velocity vectors, particles path lines, temperature contours, heat flux profiles to the furnace walls, contours of $O_2$, $CO_2$ and other species concentrations, as well as data on other important variables. Some typical results are displayed in the following figures. Flow field shown through gas phase velocity vectors in two vertical furnace central intersections is presented in fig. 5. Disturbances of the general upward flow can be seen in the vicinity of the burners. The existence of some regions with reversed flow in the furnace is predicted correctly.
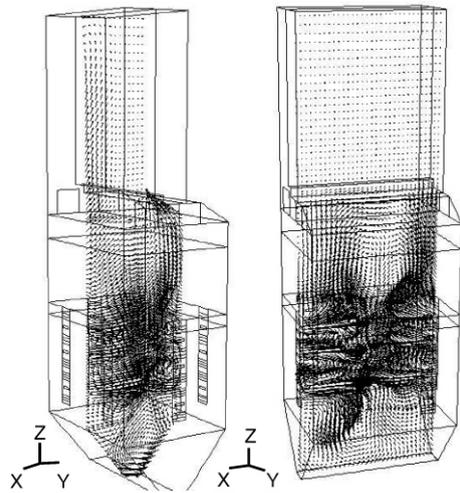
**Figure 5. Gas phase velocity vectors in central vertical cross-sections**

Simulation results of typical temperature distribution in vertical and horizontal intersections of the computational domain at boiler full load are presented in fig. 6. The plots highlight the flame shape and furnace hot spots outside the burner flame boundaries. The tangential movement of the flue ga

ses-particles mixture in the horizontal intersection at the burners' level is clearly visible, appearing as a consequence of the burners' position. Central position of the flame suggests that the temperature load of the boiler heat exchanging surfaces in the analysed operating mode is well balanced. Certain colder layer, close to the membrane walls, surrounding the warmer core gases, is very distinctive.
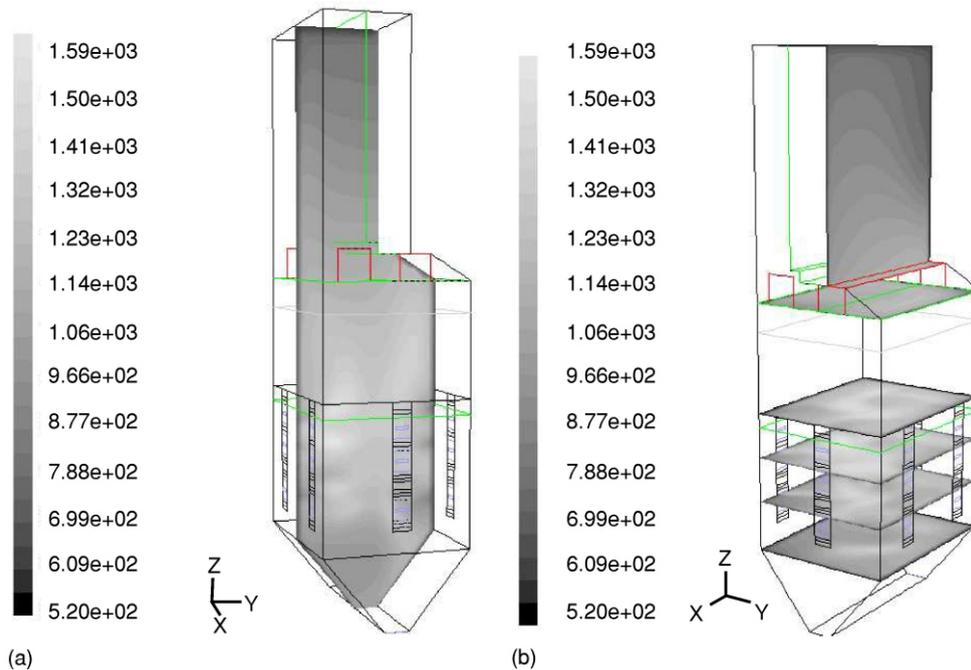


**Figure 6. Temperature fields (*T* in K) in central vertical intersection and at different horizontal levels (color image see on our web site)**

170

The most significant effect on the formation of the temperature field in the furnace is exerted by the aerodynamic of the gases flow, the kind of fuel and the operational conditions of the combustion process. An important role here plays the organisation of the flame, connected with the construction and arrangement of the burners. Temperature distribution along the furnace height, at the cross-section of the furnace and at the outlet, as well, is determined mainly by the relationship between the heat generation due to the fuel combustion, heat transfer from the flame to the heat-absorbing surfaces and aerodynamic peculiarities. In tangential coal fired boilers, the gas temperature deviation at the furnace exit could occur as the scale of the boiler becomes larger. It is commonly considered that it results from the after twirl in the furnace exit, which depends mainly on the dimensions and shape of the platen superheater, the way of the secondary air introduction and the shape of the furnace. This phenomenon can result in damage of superheaters' and reheaters' pipes. Although the investigated unit could not be treated as a large capacity boiler, according to the present simulations, temperature deviation appears to some extent in the upper part of the furnace (vertical cross-section, fig. 6b).

Very close to the coal and air inlets the temperature reaches its minimum values, as the gases are cooled by the colder input fluxes. As expected, the highest temperatures, according to the CFD predictions somewhat above 1300 °C, are detected in the furnace core, where the combustion process is the most intensive. It can be noticed that the presented numerical method slightly overestimates the expected temperature values at the furnace core. This could be attributed to the relatively simplified radiation modelling approach. The average furnace outlet temperature, which, according to the long-term experience with the boiler operation, should be 950-980 °C, is asserted with the model, with insignificant deviations. Estimation of the combustion efficiency shows almost 100% fuel conversion in the cases of 83 % and full boiler loading, with predicted unburned fuel loss below 2%, suggesting that the fuel combustion in the boiler runs successfully and is completed before the upper furnace zones.

In the present study, the uneven distribution of the fuel and air mass flow inlet between different burners is in range   25%, causing certain disturbances of the main tangential stream. For instance, minimum fuel mass flow at regime R1 is 5.44 kg/s at burner No. 6, maximum is 9.056 kg/s at burner No. 5 and the total fuel mass flow rate at the inlet is 36.11 kg/s. Predictions of path lines of coal particles, initiated from the fuel inlets of the burner No. 1 are shown in fig. 7a. The flow pattern exhibits a certain distortion due to the interchange between the gas and the solid phase. Knowing possible path lines of the fuel particles can be very important information for prediction of position where the most intensive combustion occurs. Path lines picture can also help in gaining closer insight into the reasons for appearance of incomplete combustion. Track of single coal particle released from the burner No. 4 is displayed in fig. 7b. Swirling flow field in the furnace is clearly visible.

Figure 8 depicts contours of mass fraction of oxygen in the central vertical intersection of the furnace. Profiles of $O_2$ concentration in the upper parts of the near burner regions show quite low values of $O_2$ mass fraction, which is a consequence of the equilibrium chemistry assumption inherent in the PDF model. Although, there are no available
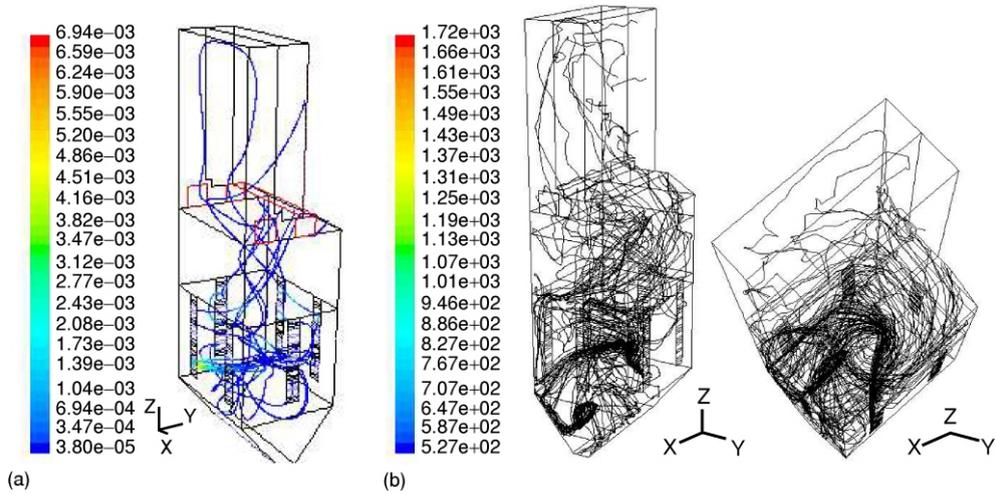
**Figure 7. (a) Path lines of coal particles streams released from the burner No. 1, and (b) traces of particles released from the burner No. 4 (color image see on our web site)**
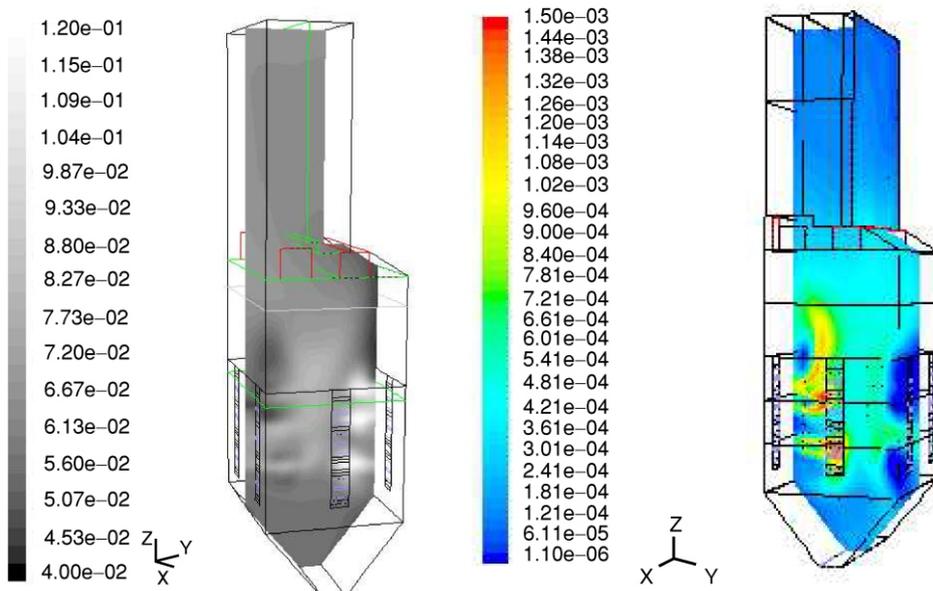


**Figure 8. Contours of oxygen mass fraction at the furnace central cross-section (color image see on our web site)**

**Figure 9. Contours of NO mass fraction at the furnace central cross-section and at the furnace exit (color image see on our web site)**

site operation records regarding the $O_2$ mass fraction at the furnace outlet, comparison to the values of excess air coefficient ahead of the air heaters (tab. 3) shows that the numerical results are close to the real values.

Present simulations include assessment of the $NO_x$ formation and reduction during the combustion process. An example of the results concerning this issue is presented in fig. 9. Since the used fuel is low calorific lignite and, consequently, furnace temperatures are moderate, appearance of thermal $NO_x$ is irrelevant and the total $NO_x$ emission, consisting mostly of fuel $NO_x$, is not very high.

Temperature and heat flux to the walls in the furnace are measured through 31 measurement ports at four levels: 13.9, 20.4, 23.0, and 26.4 m (the bottom of the furnace funnel is located approximately at elevation of 6.5 m), with aspiration pyrometer, non-cooled temperature probe and digital optical pyrometer.

Typical profiles of measured and computed temperatures from the front furnace wall in direction toward the centre, at elevation 26.4 m, are shown in fig. 10 [15]. Relatively well conformity between the CFD predictions and available field data can be noticed at the right side, but the discrepancy is considerable on the left side of the central furnace cross-section. Profiles of measured and average area-weighted temperature along the furnace height at modes R1 to R5 are displayed in fig. 11 [15]. Appearance of



**Figure 10. Temperature contours at elevation 26.4 m (approx. 20 m above the furnace bottom), mode R1: CFD-P15, CFD-P22 – model, 1.075 m from the left and right sidewall, respectively; M-P15, M-P22 – measurements, 1.075 m from the left and right sidewall**
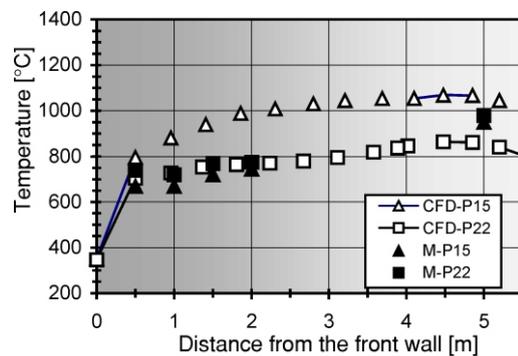
**Figure 11. Area-weighted average temperature along the furnace height: R1 to R5 – measurements; CFD-R1 to CFD-R5 – model results**
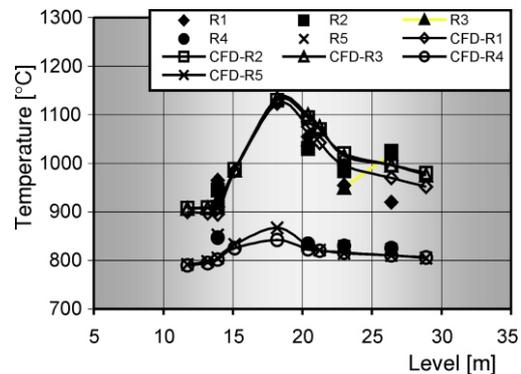
temperature peaks at approximate height of 18 m cannot be verified, neither denied with the available measurements. Figure 12 depicts area-weighted average heat flux to the walls along the furnace height, predicted with CFD and confronted with measured heat fluxes [15]. According to the simulations, maximum local heat flux values in the zone of intensive combustion don't exceed 120-150 $kW/m^2$, which is in agreement with recommendations for this type of boiler furnace. It must be noted that the averaging of the heat flux in this case is relatively rough, since the tangential burners direction causes uneven heat flux distribution in horizontal direction of the furnace walls at the burners level. Measurements are conducted at several different points on each level, and, for instance, the maximum heat flux value at elevation 13.9 m is registered at left hand side and the minimum at right and back sides.
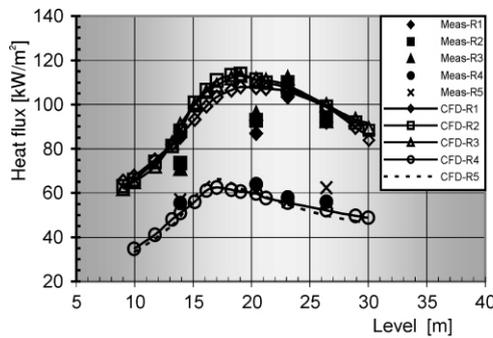


**Figure 12. Heat flux distribution along the furnace height**
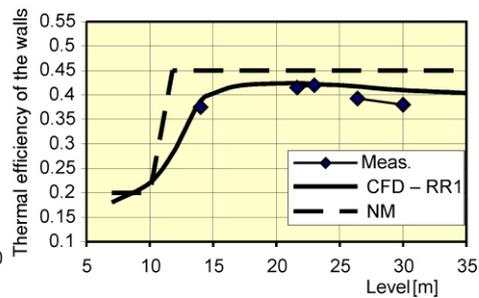
**Figure 13. Average coefficient of thermal efficiency of the furnace walls**

A change of the average thermal efficiency of the furnace walls along the boiler height is given in fig. 13 [15]. In this diagram, the results obtained by the CFD simulations are confronted to the values calculated indirectly on the basis of the heat flux and temperature measurements. For comparison, the change of the thermal efficiency of the walls according to the Normative Method of the CKTI (according to [22]) is presented in the same figure.

Combustion efficiency in the modes R1-R3, according to the measurements and CFD simulations, is illustrated with fig. 14 [15]. The variation of the combustion efficiency as a function of coal sieve analysis is presented in fig. 15 [15, 16]. Results are obtained with the numerical model, analysing cases when the coal dust mean diameter is $d_{pm}$ = 110 and 140 m. The influence of the better coal grinding to the minimisation of heat losses caused by incomplete combustion is obvious.

174
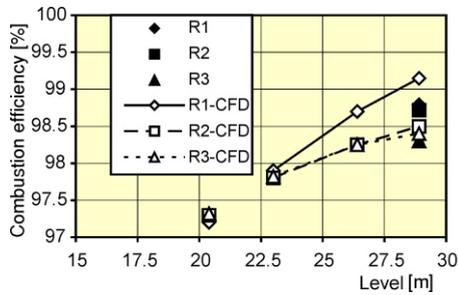
**Figure 14. Combustion efficiency along the furnace in the modes R1, R2, and R3**
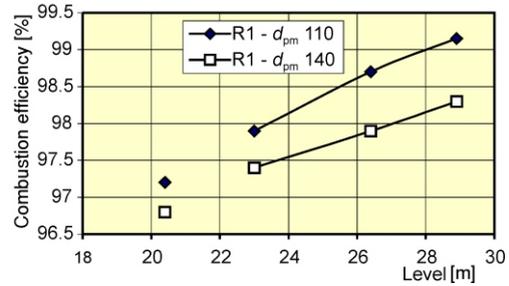
**Figure 15. Combustion efficiency as function of coal sieve characteristics at $d_{pm}$ = 110 and 140   m**

Figure 16 illustrates the impact of introduction of OFA ports for secondary air to the concentration of $NO_x$ in the flue gases [15, 16]. Scheme in fig. 16a shows the presumed position of the OFA port above the burner. Profiles of mass fractions of CO and $NO_x$ in the central vertical furnace intersection in mode R1 with implemented OFA system for secondary air are given in fig. 17. The concentrations of both, CO and $NO_x$, are substantially lower than in the case without OFA ports.
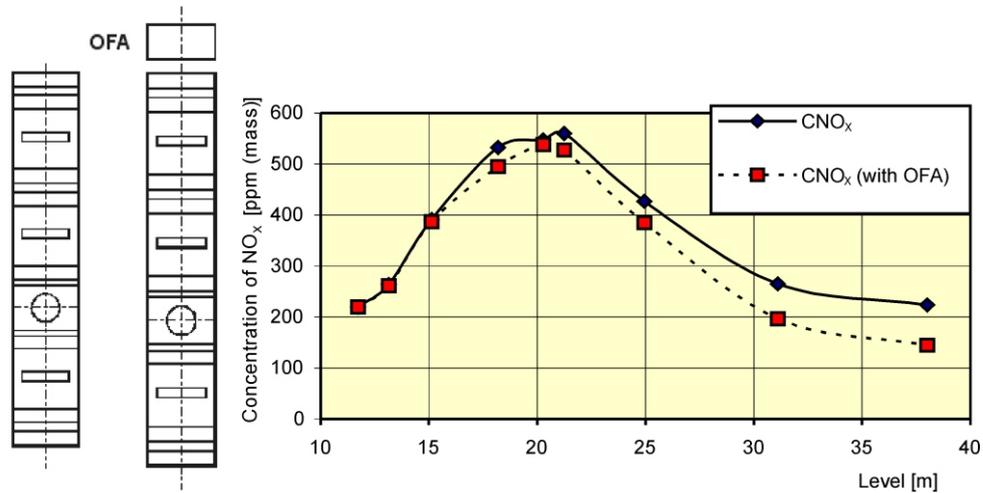


**Figure 16. (a) Position of OFA port; (b) Concentration of $NO_x$ along the furnace height – mode R1 with and without OFA system implemented**
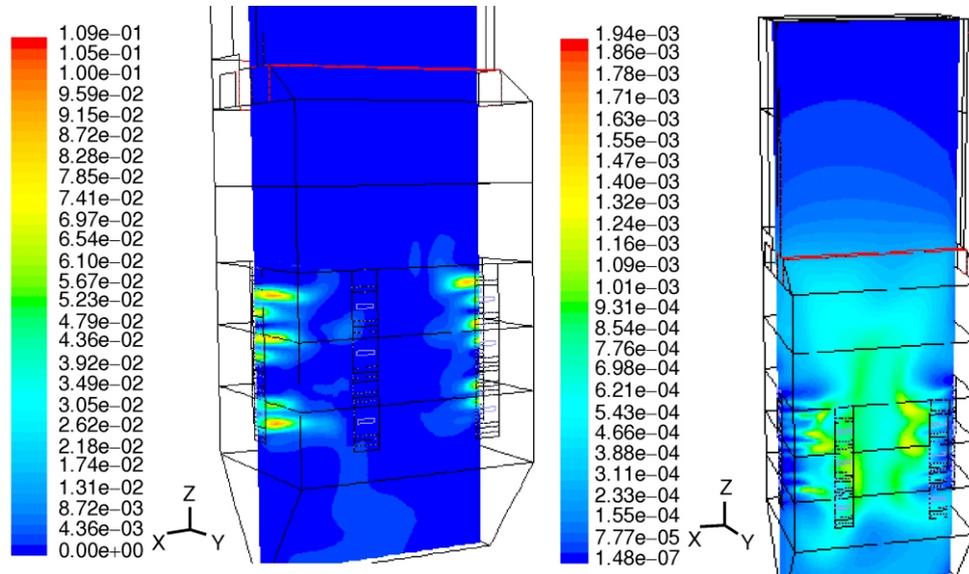
**Figure 17. Profiles of mass fractions of CO and NO in central vertical furnace intersection in the mode R1 with OFA system for secondary air implemented (color image see on our web site)**

Finally, fig. 18 is an illustrative example of the temperature profile in the mode R1 with implemented OFA system for secondary air introduction. The temperature in the intersection behind the platen superheater is much evenly distributed in the presumed case when the OFA system is implemented, compared to the case presented in fig. 6b. The velocity direction is supposed to be normal to the furnace walls, which additionally contributes to the minimisation of temperature deviation.
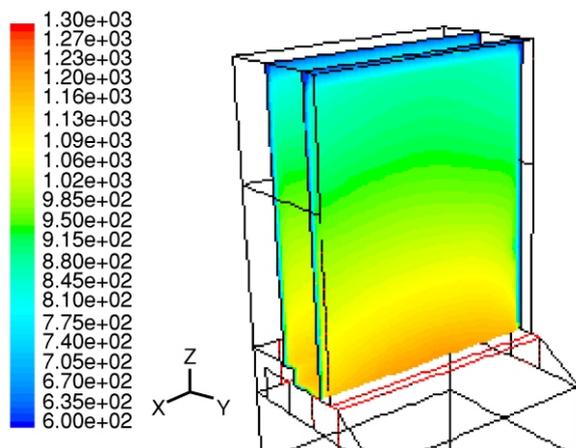


**Figure 18. Temperature profile in the intersection behind the platen superheater in the mode R1 with implemented OFA system for secondary air (color image see on our web site)**

The described CFD method gives a possibility to investigate the operation of the boiler in various conditions, with different load, as well as with redistribution of coal and air mass flow at the inlets, which would lead to certain changes of the flame position and other parameters. The procedure discussed in the article and applied here to large boiler furnace has wide band assertion applicability. The justification for this resides in the variety of processes and phenomena, which the CFD has already been shown to be able to handle. Current and future work in this field is focused on further simulations of the boiler operation with: varied burners' loading, coal of various size distribution, over-fire-air system implemented, calculations of $NO_x$ emission and predictions of aerodynamics and thermal behaviour of gas-solids mixture in the near-burner region.

## Conclusions

The paper presents methodology used to numerically model furnace processes of a tangential pulverised coal-fired power boiler, based on computational fluid dynamics and computational thermal analysis. On a basis of comparison with available site records a conclusion can be drawn that the model produces realistic insight into the furnace processes. Values of temperature and heat flux are in expected limits, typical for this boiler type and for the coal used and, generally, they follow the trend line of measurements. The model slightly overestimates the temperature values at the furnace core, but relatively well describes the two-phase gas-solid flow field, mostly determined by the tangential disposition of the burners.

Simulation results concerning the furnace walls thermal efficiency and combustion efficiency also show good correspondence with the plant data. Predictions on CO and $NO_x$ concentrations, both with and without OFA system, could not be verified with available field data, but the obtained values are quite reasonable and in line with the previous experience with similar boiler designs.

## Nomenclature

$a$ – absorption coefficient, [–]
$a_p$ – equivalent absorption coefficient due to presence of particulates, [–]
$C$ – linear-anisotropic phase function coefficient, [–]
$C_{1\varepsilon}$ – constant in the $k$-$\varepsilon$ turbulence model, (= 1.44), [–]
$C_{2\varepsilon}$ – constant in the $k$-$\varepsilon$ turbulence model, (= 1.92), [–]
$d_p$ – particle diameter, [m]
$E_p$ – equivalent particle emissivity, [–]
$G$ – incident radiation, [W/m$^2$]
$G_w$ – incident wall radiation, [W/m$^2$]
$I$ – total radiation intensity, [W/m$^2$]
$k$ – turbulence kinetic energy, [m$^2$/s$^2$]
$n$ – refractive index, [–]
$q_r$ – radiation flux, [W/m$^2$]
$q_{rw}$ – incident radiation flux at wall, [W/m$^2$]

**r** – position vector, [–]
$r_g$ – recirculating factor, [–]
$s$ – path length, [m]
**s** – direction vector, [–]
**s'** – scattering direction vector, [–]
$T$ – temperature, [K]
$T_w$ – wall temperature, [K]

*Greek symbols*

$\Gamma$ – parameter defined through the equivalent absorption coefficient $a_p$ and the equivalent
      particle scattering factor $\sigma_p$, eq. (4)
$\varepsilon$ – turbulence kinetic energy dissipation rate, [m$^2$/s$^3$]
$\varepsilon_\omega$ – wall emissivity, [–]
$\sigma$ – Stefan-Boltzmann constant, (= 5.672 10$^{-8}$ W/m$^2$K$^4$)
$\sigma_k$ – kinetic energy constant in the transport equations, [–]
$\sigma_p$ – equivalent particle scattering factor, [–]
$\sigma_s$ – scattering coefficient, [–]
$\sigma_\varepsilon$ – kinetic energy dissipation rate constant in the transport equations, [–]
$\Phi$ – phase function, [–]
$\Omega'$ – solid angle, [sterad]

# References

[1] Fiveland, A. W., Wessel, A. R., Numerical Model for Predicting Performance of Three-Dimensional Pulverized-Fuel Fired Furnaces, *Journal of Eng. for Gas Turbines and Power, 110* (1988), 1, pp. 117-126

[2] Risio, B., Schnell, U., New Numerical Methods for the Description of Phenomena Occurring in Tangentially Fired Pulverised Coal Boilers, EU Project *Performance Prediction in Advanced Coal Fired Boilers*, Contract No JOF3-CT95-0005, Stuttgart, Germany, 1998

[3] Xu, M., Azevedo, J. L. T., Carvalho, M. G., Modelling of the Combustion Process and NO$_x$ Emission in a Utility Boiler, *Fuel, 79* (2000), 13, pp. 1611-1619

[4] Fan, J., Qian, L., Ma, Y., Sun, P., Cen, K., Computational Modeling of Pulverized Coal Combustion Processes in Tangentially Fired Furnaces, *Chemical Engineering Journal, 81* (2001), pp. 261-270

[5] Jones, J. M., Pourkashanian, M., Williams, A., Chakraborty, R. K., Sykes, J., Laurence, D., Modelling of Coal Combustion Processes – a Review of Present Status and Future Needs, *Proceedings*, 15$^{th}$ Annual International Pittsburgh Coal Conference, Pittsburgh, PA, USA, 1998, pp. 1-20

[6] Eaton, A. M., Smoot, L. D., Hill, S. C., Eatough, C. N., Components, Formulations, Solutions, Evaluation and Application of Comprehensive Combustion Models, *Progress in Energy and Combustion Science, 25* (1999), 4, pp. 387-436

[7] Hill, S. C., Smoot, L. D., A Comprehensive Three-Dimensional Model for Simulation of Combustion Systems, PCGC-3, *Energy & Fuels, 7* (1993), 6, pp. 874-883

[8] Jessee, J. P., Fiveland, W. A., Howell, L. H., Colella, P., Pember, R. B., An Adaptive Mesh Refinement Algorithm for the Discrete Ordinates Method, RDTPA 96-14, 1996 National Heat Transfer Conference, Houston, Tex., USA, 1996

[9] Bermudez de Castro, A., Ferin, J. L., Modelling and Numerical Solution of a Pulverized Coal Furnace, *Proceedings*, 4$^{th}$ International Conference on Technologies and Combustion for Clean Environment, Lisbon, Portugal, 1997, paper 33.1, pp. 1-9

178

[10] Zhou, L. X., Li, L., Li, R. X., Zhang, J., Simulation of 3-D Gas-Particle Flows and Coal Combustion in a Tangentially Fired Furnace Using a Two-Fluid-Trajectory Model, *Powder Technology, 125* (2002), 2-3, pp. 226-233

[11] Schnell, U., Numerical Modelling of Solid Fuel Combustion Processes Using Advanced CFD-Based Simulation Tools, *International Journal of Progress in Computational Fluid Dynamics, 1* (2001), 4, pp. 208-218

[12] Knaus, H., Schnell, U., Hein, K. R. G., On the Modelling of Coal Combustion in a 550 MWel Coal-Fired Utility Boiler, *International Journal of Progress in Computational Fluid Dynamics, 1* (2001), 4, pp. 194-207

[13] Yin, C., Caillat, S., Harion, J. L., Baudoin, B., Perez, E., Investigation of the Flow, Combustion, Heat-Transfer and Emissions from a 609 MW Utility Tangentially Fired Pulverized Coal Boiler, *Fuel, 81* (2002), 8, pp. 997-1006

[14] Ratzel, A. C., Howell, J. R., Two-Dimensional Radiation in Absorbing-Emitting Media Using the P-N Approximation, *Journal of Heat Transfer,* Transactions of the ASME, Vol. 105 1983, pp. 333-340

[15] Filkoski, R. V., Modelling of Thermal Processes and Optimisation of Energetic-Environmental Characteristics of Modern Boiler Plants, Ph. D. thesis, Faculty of Mech. Eng., University "Sts Cyril & Methodius", Skopje, Republic of Macedonia, 2004

[16] Filkoski, R. V., Petrovski, I. J., Karas, P., CFD/CTA Modelling Suggests Ways Towards Lower Emission from Pulverised Coal Combustion, International Symposium Moving Towards Zero-Emission Plants, Leptokarya Pieria, Greece, 2005

[17] ***, Fluent User's Guide, Fluent Inc., Lebanon, NH, USA, 1998, 2000

[18] Kuo, K. K., Principles of Combustion, John Wiley & Sons, New York–Chichester–Brisbane–Toronto–Singapore, 1986

[19] Siegel, R., Howell, J. R., Thermal Radiation Heat Transfer, Hemisphere Publ. Corp., Washington D. C., 1992

[20] Khalil, E. E., Modelling of Furnaces and Combustors, Abacus Press, Tunbridge Wells, Kent, GB, 1982

[21] Hottel, H. C., Sarofim, A. F., Radiative Transfer, McGraw-Hill, New York, USA, 1967

[22] Blokh, A. G., Heat Transfer in Steam Boiler Furnaces, Hemisphere Publ., London, 1988

Authors' addresses:

*A. V. Filkoski, I. J. Petrovski*
Faculty of Mechanical Engineering
University "Sts. Cyril & Methodius"
P. O. Box 464, 1000 Skopje, Republic of Macedonia

*P. Karas*
RAFAKO S. A., 33 Lakowa
St. 33, 47-400 Raciborz, Poland

Corresponding author (R. V. Filkoski):
E-mail: rfilko@mf.ukim.edu.mk